AGU PUBLICATIONS

Water Resources Research

RESEARCH ARTICLE
10.1002/2014WR016273

Key Points:
- TRMM-PR and 95 stations describe rainfall contrasts in Amazon-Andes transition
- Rainfall hotspots extreme events are related to synoptic atmospheric circulation
- Rainfall day-to-day variability is associated with cross-equatorial winds

Supporting Information:
- Supporting Information S1

Correspondence to:
J. C. Espinoza,
jhan-carlo.espinoza@igp.gob.pe

Citation:
Espinoza, J. C., S. Chavez, J. Ronchail, C. Junquas, K. Takahashi, and W. Lavado (2015), Rainfall hotspots over the southern tropical Andes: Spatial distribution, rainfall intensity, and relations with large-scale atmospheric circulation, *Water Resour. Res.*, *51*, 3459–3475, doi:10.1002/2014WR016273.

Received 11 AUG 2014
Accepted 23 MAR 2015
Accepted article online 17 APR 2015
Published online 11 MAY 2015

Rainfall hotspots over the southern tropical Andes: Spatial distribution, rainfall intensity, and relations with large-scale atmospheric circulation

Jhan Carlo Espinoza[1], Steven Chavez[1], Josyane Ronchail[2], Clémentine Junquas[1,3], Ken Takahashi[1], and Waldo Lavado[4]

[1]Subdirección de Ciencias de la Atmósfera e Hidrósfera (SCAH), Instituto Geofísico del Perú, Lima, Peru, [2]Univ. Paris Diderot, Sorbonne Paris Cité, UMR Locean (Sorbonne Universités-UPMC-, CNRS, IRD, MNHN), France, [3]IRD/UJF-Grenoble 1/CNRS/G-INP, LTHE UMR 5564, Grenoble, France, [4]Dirección General de Hidrología (DGH), Servicio Nacional de Meteorología e Hidrología, Peru

Abstract The Andes/Amazon transition is among the rainiest regions of the world and the interactions between large-scale circulation and the topography that determine its complex rainfall distribution remain poorly known. This work provides an in-depth analysis of the spatial distribution, variability, and intensity of rainfall in the southern Andes/Amazon transition, at seasonal and intraseasonal time scales. The analysis is based on comprehensive daily rainfall data sets from meteorological stations in Peru and Bolivia. We compare our results with high-resolution rainfall TRMM-PR 2A25 estimations. Hotspot regions are identified at low elevations in the Andean foothills (400–700 masl) and in windward conditions at Quincemil and Chipiriri, where more than 4000 mm rainfall per year are recorded. Orographic effects and exposure to easterly winds produce a strong annual rainfall gradient between the lowlands and the Andes that can reach 190 mm/km. Although TRMM-PR reproduces the spatial distribution satisfactorily, it underestimates rainfall by 35% in the hotspot regions. In the Peruvian hotspot, exceptional rainfall occurs during the austral dry season (around 1000 mm in June–July–August; JJA), but not in the Bolivian hotspot. The direction of the low-level winds over the Andean foothills partly explains this difference in the seasonal rainfall cycle. At intraseasonal scales in JJA, we found that, during northerly wind regimes, positive rainfall anomalies predominate over the lowland and the eastern flank of the Andes, whereas less rain falls at higher altitudes. On the other hand, during southerly regimes, rainfall anomalies are negative in the hotspot regions. The influence of cross-equatorial winds is particularly clear below 2000 masl.

1. Introduction

The eastern Andes/western Amazon transition is the richest region in the world in terms of biodiversity [*Myers et al.*, 2000]. This region, also the rainiest region in the Amazon basin, is characterized by complex rainfall distribution that is the result of the interactions between large-scale humidity transport and topography [*Killeen et al.*, 2007]. Intense rainfall on the eastern flank of the Andes causes high erosion rates, with maximum values over the southern tropical Andes, where climate variability is the main factor that controls erosion [*Pepin et al.*, 2013; *Lowman and Barros*, 2014]. Intense rainfall also causes flooding, which can result in loss of lives and of infrastructure and consequently have a major impact on important economic activities including agriculture and tourism. In the austral summer of 2010, flooding in the Cusco region stranded tourists in Machu Picchu for several days and caused US$250 million in losses [*Lavado et al.*, 2010; *El Comercio*, 2010]. In January 2014, extreme rainfall in the Andean piedmont over the southern part of the Peruvian and Bolivian Amazon [*Espinoza et al.*, 2014] affected about 9000 people in Peru and 24,000 families in Bolivia.

The atmospheric circulation in tropical South America is characterized by easterly trade winds, which transport moisture from the Atlantic Ocean and from the central Amazon region toward the eastern Andes. When humidity reaches the Andes, the flow becomes anticyclonic and forms an "aerial river" flowing parallel to the Andes [*Arraut and Satyamurty*, 2009; *Póveda et al.*, 2014] toward the southern Amazon and the subtropical region of South America [*Paegle and Mo*, 1997; *Byerle and Peagle*, 2002; *Berbery and Barros*, 2002]. Indeed, the topographic minimum between the Andes and the Brazilian plateau forms a corridor

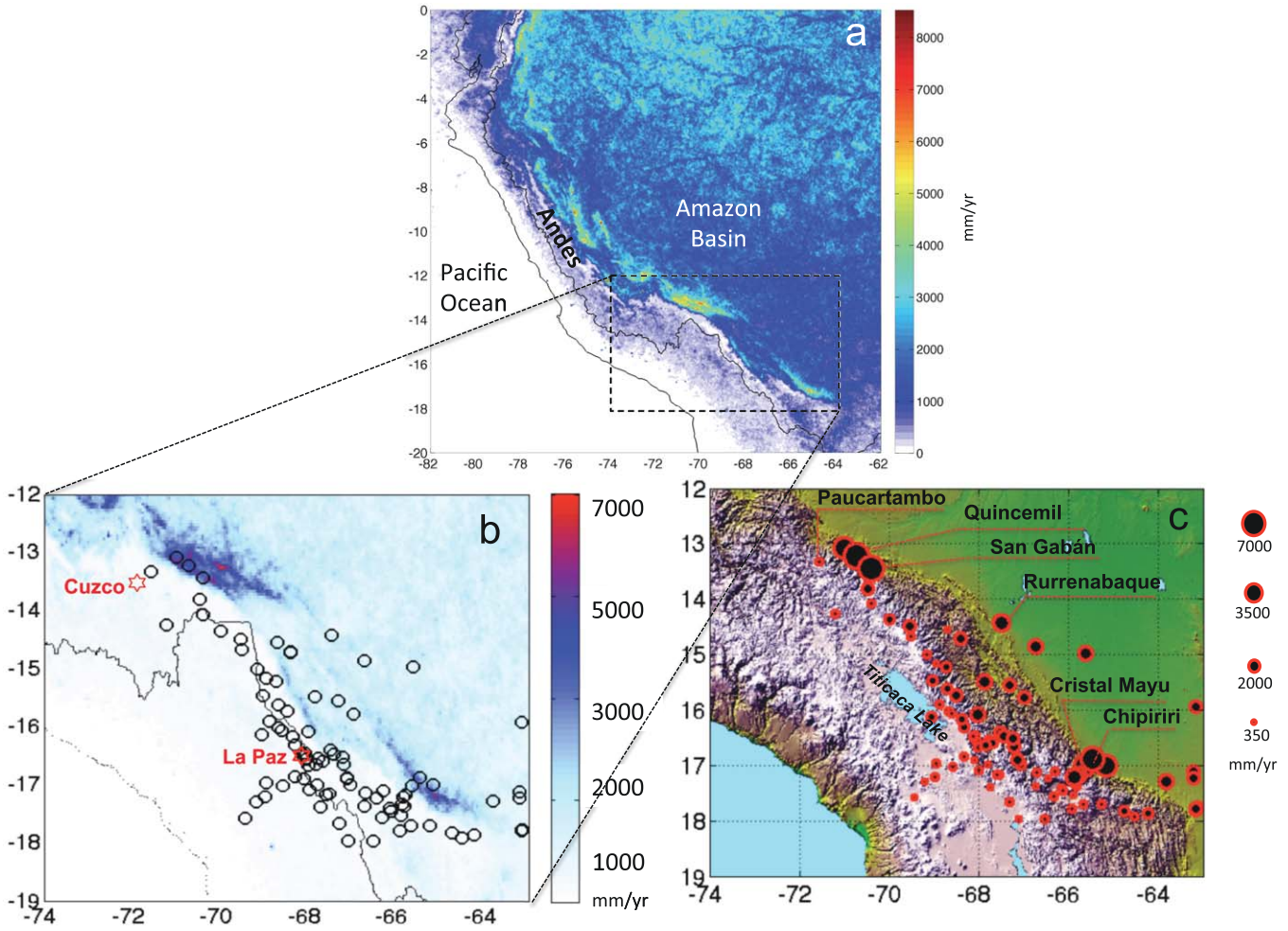

Figure 1. (a) Mean annual rainfall in western South America (mm/yr, 1998–2012) estimated using TRMM PR 2A25. (b) Meteorological stations (black circles) and mean annual rainfall in mm/yr from Figure 1a. The limits of the Amazon basin and the main towns are indicated. (c) The size of the circles represents the historical mean annual rainfall (mm/yr) at each station (1975–2005). Topography is represented using SRTM at 1 km resolution. All the meteorological stations mentioned in the text are indicated.

where the so-called South American low-level jet (SALLJ), a high-speed core of moist wind is found [*Berri and Inzunza*, 1993; *Saulo et al*., 2000; *Marengo et al*., 2004; *Grimm and Tedeschi*, 2009]. The tropical Andes have a blocking effect on this flow of humidity resulting in orographically anchored precipitation hotspots on the exposed flanks [*Figueroa and Nobre*, 1990; *Falvey and Garreaud*, 2005; *Espinoza et al*., 2009, *Póveda et al*., 2014]. This effect results in localized rainfall maxima over the eastern Andes, from Colombia to Bolivia (Figure 1a) [*Petersen et al*., 2002; *Bookhagen and Strecker*, 2008; *Nesbitt and Anders*, 2009; *Romatschke and Houze*, 2010].

Recently, high-resolution mapping of rainfall distribution became possible using remote sensing and showed that the strongest orographic intensification is localized at along-slope scales of 5–10 km [*Bookhagen and Strecker*, 2008; *Nesbitt and Anders*, 2009]. Results obtained during the high-resolution Tropical Rainfall Measurement Mission (TRMM) Precipitation Radar (PR) data suggest that the Andean relief exerts first-order control over orographic rainfall [*Bookhagen and Strecker*, 2008]. What is more, strong precipitation gradients are observed with relatively small ($<$ 1000 m vertically) topographic differences, with the upper limit for high precipitation (3000 mm/yr) at around 3000 m [*Espinoza et al*., 2009]. On the other hand, quantitative rainfall estimations based on remote sensing in the Andes region are subject to major errors, that can reach 50% underestimation, implying that for hydrological applications, these data need to be calibrated with in situ measurements [*Condom et al*., 2011, *Scheel et al*., 2011; *Zulkafli et al*., 2014]. Underestimations are also observed in the Amazon lowlands, although to a lesser extent [*Getirana et al*., 2011; *Buarque et al*., 2010].

Over the southern tropical Amazon and Andes (south of 10°S), precipitation occurs predominantly during the austral summer linked to the mature phase of the South American monsoon system (SAMS) [*Zhou and Lau*, 1998; *Vera et al*., 2006], which feeds into the South Atlantic Convergence Zone (SACZ) [*Kodama*, 1992; *Lenters and Cook*, 1995; *Liebmann et al*., 1999] and the Bolivian High [*Aceituno and Montecinos*, 1993, *Garreaud*, 2000, *Garreaud et al*., 2003]. In contrast, between April and September there is a dry season, which is particularly intense over the Andes and the Altiplano linked to the weakening transport of humidity and to the onset of a westerly jet in the upper troposphere [e.g., *Figueroa and Nobre*, 1990; *Garreaud et al*., 2003; *Espinoza et al*., 2009]. Several authors analyzed the role of atmospheric circulation in seasonal rainfall variability in the southern Andes piedmont. Their results revealed that the rainfall hotspots (e.g., Cusco Amazon and Chapare in Bolivia) remain humid throughout the year and that estimated evapotranspiration did not exceed precipitation in any month [*Hijmans et al*., 2005; *Killeen et al*., 2007]. In hotspot regions, the convergence of humidity and intense rainfall also occur in austral winter, linked to southeastern trade winds enhanced by the strengthening of the South Atlantic anticyclone [e.g., *Póveda et al*., 2014].

At the intraseasonal timescale, tropical South America is subject to major spatiotemporal variations in rainfall [*Satyamurty et al*., 1998]. For instance, cross-equatorial low-level flow over the western Amazon has been shown to be closely linked with precipitation, and a southerly flow is generally associated with precipitation north of the equator [*Wang and Fu*, 2002]. The fluctuations in rainfall in austral summer are partially linked to the marked spatial and temporal variability of the SACZ [*Carvalho et al*., 2002a, 2002b; *Liebmann et al*., 1999, 2004; *Jones and Carvalho*, 2002; *De Souza and Ambrizzi*, 2006] and have impacts on mesoscale activity [*Petersen et al*., 2002]. Recent studies also evidenced the well-organized temporal evolution of the intraseasonal atmospheric circulation in the Amazon basin in a cycle of seven phases or circulation patterns [*Espinoza et al*., 2012, 2013]. These authors also demonstrated that the northward propagation of rainfall from the La Plata basin to northwest Amazon is associated with alternating negative and positive geopotential anomalies over the southern Pacific and Atlantic oceans and over the South American continent, which drive the northward progression of cold and dry air masses from the south, destabilizing the tropical atmosphere by forcing the ascent of warm and moist air. In the Andean region and in the Altiplano, summer precipitation is partly modulated by the local boundary layer moisture and upward zonal wind [*Garreaud*, 2001; *Minvielle and Garreaud*, 2011]. However, the analysis of the modulation of intraseasonal rainfall and its relationship with atmospheric circulation in the Andean piedmont, including hotspot regions, is still lacking.

To summarize, previous studies based on high-resolution rainfall estimations have substantially improved our knowledge of the spatial distribution of rainfall in the eastern part of the Andes and its seasonality. The present work aims to build on our prior knowledge and has two main goals. The first goal is to provide an in-depth analysis of the spatial distribution, variability, and intensity of rainfall in the Andes/southern Amazon transition at seasonal and intraseasonal time scales. This analysis is based on comprehensive observed daily rainfall data sets from Peru and Bolivia that include information from the rainfall hotspots in Peru and Bolivia (Figure 1b). In addition, we compare our results with TRMM-PR 2A25 high-resolution rainfall estimations [*Nesbitt and Anders*, 2009]. The second goal is to analyze the relationship between extreme intraseasonal dry and wet events over this region and regional atmospheric circulation. Particular emphasis is given to the Peruvian and Bolivian rainfall hotspots. Whereas previous studies analyzed the relationship between northerly and southerly regimes and rainfall using information from Amazonian lowlands [e.g., *Wang and Fu*, 2002; *Espinoza et al*., 2012], we evaluate the influence of wind regimes on rainfall in the Peruvian hotspot and in the eastern part of the Andes.

Rainfall and atmospheric data are presented in section 2. The spatial distribution of rainfall in the hotspots, their relation to altitude, and the intensity of rainfall are analyzed in section 3. The seasonal rainfall cycle over this region is discussed in section 4. In section 5, we analyze and discuss the interactions between the intraseasonal atmospheric circulation and both extreme wet and dry winter events. Our conclusions and final remarks are presented in section 6.

2. Rainfall and Atmospheric Data Sets

We used daily rainfall observations from 13°S to 18°S and 62°W to 72°W in the southern Andes-Amazon region for the period 1970–2005 (Figure 1), covering an altitudinal gradient from 160 to 4700 masl (for more details see supporting information). The data comes from the hydrometeorological services

(SENAMHI) in Peru and Bolivia. The quality of the rainfall data was first checked at interannual timescales using the Regional Vector Method [*Espinoza et al*., 2009]. At a daily time step, outliers were identified and compared with values recorded at nearby meteorological stations and those that did not match data from neighboring stations were discarded. Rainfall data recorded at stations with less than 20% of missing values were finally selected giving a total of 95 rainfall stations used in this work. To complete this information, Tropical Rainfall Measuring Mission satellite Precipitation Radar (TRMM-PR) rainfall estimations were used to describe the spatial distribution of the rainfall over regions where in situ observations are lacking. We used version 7 of the data set for the period 1998–2012. The climatology was constructed from rainfall information taken from the 2A25 product remapped into Cartesian coordinates using bilinear interpolation, with a horizontal resolution of 5 km. Information from TRMM products is available at http://disc.sci.gsfc.nasa.gov/precipitation/documentation/TRMM_README.

Large-scale atmospheric circulation is described using daily values from the 40 year European Centre for Medium-Range Weather Forecast (ECMWF) reanalysis (ERA–40) [*Uppala et al*., 2005] and ERA-interim reanalysis [*Dee et al*., 2011]. ERA-40 and ERA-Interim 850 hPa zonal and meridional winds and geopotential height were also analyzed. ERA-40 data are available at a grid resolution of $2.5^\circ \times 2.5^\circ$ (http://data-portal.ecmwf.int/ data/d/era40_daily) and are useful to evaluate large-scale atmospheric circulation. ERA-Interim data are available at a grid resolution of $0.25^\circ \times 0.25^\circ$ (http://apps.ecmwf.int/datasets/data/interim_full_daily/) and make it possible to describe more details concerning the Andes/Amazon transition. To characterize the intraseasonal variability of the atmospheric circulation, cross-equatorial wind regimes were defined for the 1970–2005 period [*Wang and Fu*, 2002]. Northerly and southerly regimes were computed using area-averaged daily 850 hPa meridional winds from ERA-40 reanalysis (5°S–5°N, 65°–75°W) and from winds recorded at Iquitos meteorological station in the Peruvian Amazon (3.75°S, 73.25°W).

3. Spatial Distribution of Rainfall Over the Southern Tropical Andes

A line corresponding to rainfall above 3000 mm/yr roughly outlines the eastern Andes (Figure 1a) but the spatial distribution of rainfall is complex and some very rainy hotspots are located in the eastern foothills of the southern tropical Andes (Figure 1b). Rainfall of up to 7000 mm/yr is estimated from TRMM-PR and is confirmed by rain gauges. Indeed, mean values recorded at Quincemil (770 masl) and San Gabán (640 masl) meteorological stations reach 6600 and 5900 mm/yr, respectively (Figure 1c). Further south, Chipiriri (410 masl) and Cristal Mayu (880 masl) stations in the Bolivian hotspot record lower values around 4800 and 4100 mm/yr, respectively. In conclusion, we recognize two "hotspot regions" defined by Quincemil and San Gabán stations (in the north) and Chipiriri and Cristal Mayu stations (in the south) over the Bolivian and Peruvian Andes/Amazon transition. Rainfall values in these regions are extremely high considering that estimated mean rainfall in the whole Amazon basin is 2200 mm/yr [*Marengo and Nobre*, 2001; *Espinoza et al*., 2009]. In the Bolivian Amazon, east of the rainfall hotspot, rainfall is considerably lower than that recorded at Chipiriri and Cristal Mayu meteorological stations. For instance, Rurrenabaque station record 2200 mm/yr (Figure 1c). This information confirms a difference of up to a factor of 3 between rainfall in the Amazon lowlands and in the hotspot regions. Toward the Andean and Altiplano regions, rainfall decreases to 300 mm/yr (e.g., 530 mm/yr recorded at Paucartambo meteorological station; Figure 1c).

Figure 2 shows more details on the rainfall distribution in the Andes/Amazon transition with an altitudinal profile from the hotspot regions to the Andean meteorological stations. The northern profile (in Peru) is oriented northwest-southeast, which corresponds to the main direction of the low-level wind, then north-south following the San Gabán River valley. The southern profile (in Bolivia) is oriented northeast-southwest from the Bolivian Amazon to the eastern Andes. In Peru, the maximum rainfall values ($\geq$ 6000 mm/yr) are recorded at 600 masl (Quincemil and San Gabán stations), while rainfall decreases (4000 mm/yr) in nearby regions at higher altitudes (Pilcopata, 900 masl). A dramatic decrease in rainfall is observed westward, in particular above 3000 masl (Figure 2b). In the Bolivian hotspot, maximum rainfall ($\sim$5000 mm/yr) is recorded at Chipiriri station (410 masl), while rainfall is slightly lower (4000 mm/yr) in higher regions nearby (e.g., Cristal Mayu; 900 masl). Figures 2b and 2c show that the eastern flank of the altitudinal profile, oriented toward humid winds, is characterized by very wet conditions, even at high altitudes. For instance, at Corani meteorological station (3240 masl), mean annual rainfall reach 2540 mm/yr (Figure 2c). This amount of rainfall is rarely recorded above 3000 masl in the Andean region. Rainfall decreases dramatically over the

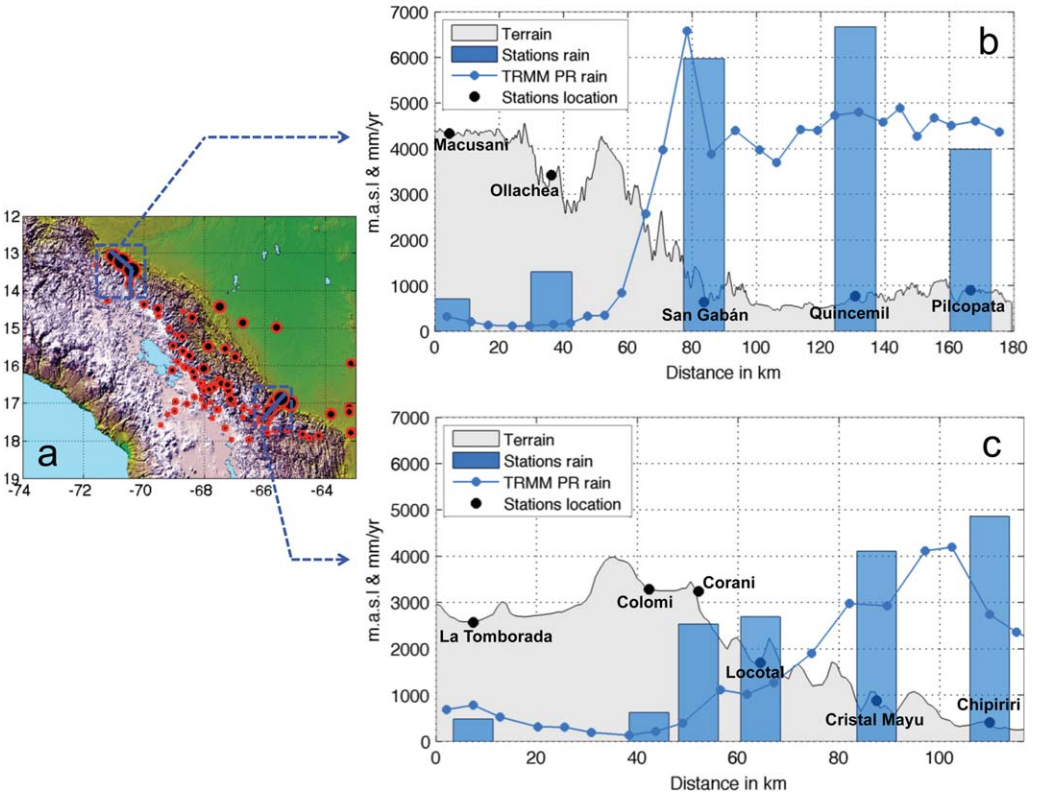

Figure 2. (a) As in Figure 1c. The blue line represents the axis of the cross-section illustrated in Figures 2b and 2c. (b) Topographical profile (gray) and total annual rainfall from Macusani to Pilcopata meteorological stations (Peru). The x axis represents the horizontal distance and the y axis the altitude (masl) and the mean total rainfall (mm/yr) from observations (blue bars) and TRMM PR-2A25 (blue line). (c) As in Figure 2b but for the La Tamborada-Chipiriri profile in Bolivia.

highlands and on the leeward side of the Andes (e.g., Colomi, La Tamborada in the southern profile, Ollachea and Macusani stations in the northern profile). For instance, between Corani meteorological station (on the windward side) and Colomi station (on the leeward side), both situated at around 3250 masl, rainfall decreases from 2540 to 628 mm/yr over a distance of 10 km (Figure 2c). These values represent an exceptional spatial gradient of 190 mm/km, confirming that windward and leeward conditions play a key role in explaining the spatial distribution of rainfall over the eastern Andes.

Rainfall estimated by TRMM-PR 2A25 in Figure 2 also shows maximum rainfall in the hotspot regions with values of around 4500 and 3500 mm/yr in the Peruvian and Bolivian hotspots, respectively. Peak TRMM-PR rainfall estimations are located on the windward side of the mountains, for instance, near San Gabán and between Chipiriri and Cristal Mayu meteorological stations. However, TRMM-PR underestimates total annual rainfall in this region by approximately 35% in the hotspot region (Quincemil, San Gabán, and Chipiriri stations), and shows an even bigger underestimation over the highlands (up to 80% in Ollachea, Corani, and Colomi stations). Thus, while TRMM-PR can adequately describe the main features of the spatial distribution of rainfall in the Andean region (e.g., Figures 1a and 1b), in situ observations are indispensable for an in depth analysis of rainfall over the hotspot regions. These results underline the need to validate TRMM-PR estimations over the Andean mountains [e.g., *Chavez*, 2013].

Our analysis of rainfall occurrence over this region shows that rainy days (i.e., days with more than 1 mm of rain) occur at least 40% of the time in the hotspot regions during the 1970–2005 period (Figure 3a), with the highest percentage in Quincemil (66%) and Cristal Mayu (60%). Over the Amazon region and over the eastern flank of the Andes, the percentage falls to 20% and 40%, with the exception of some meteorological stations located leeward. A rapid transition occurs toward the Altiplano, where only 12%–20% of rainy days are recorded (Figure 3a). The frequency of rainy days thus explains annual rainfall over this region reasonably well. The coefficient of correlation between annual rainfall and the percentage of days with rainfall >1 mm is 0.82 ($N = 95$, $p \leq 0.001$). The frequency of rainy days thus only explains 66% of the spatial

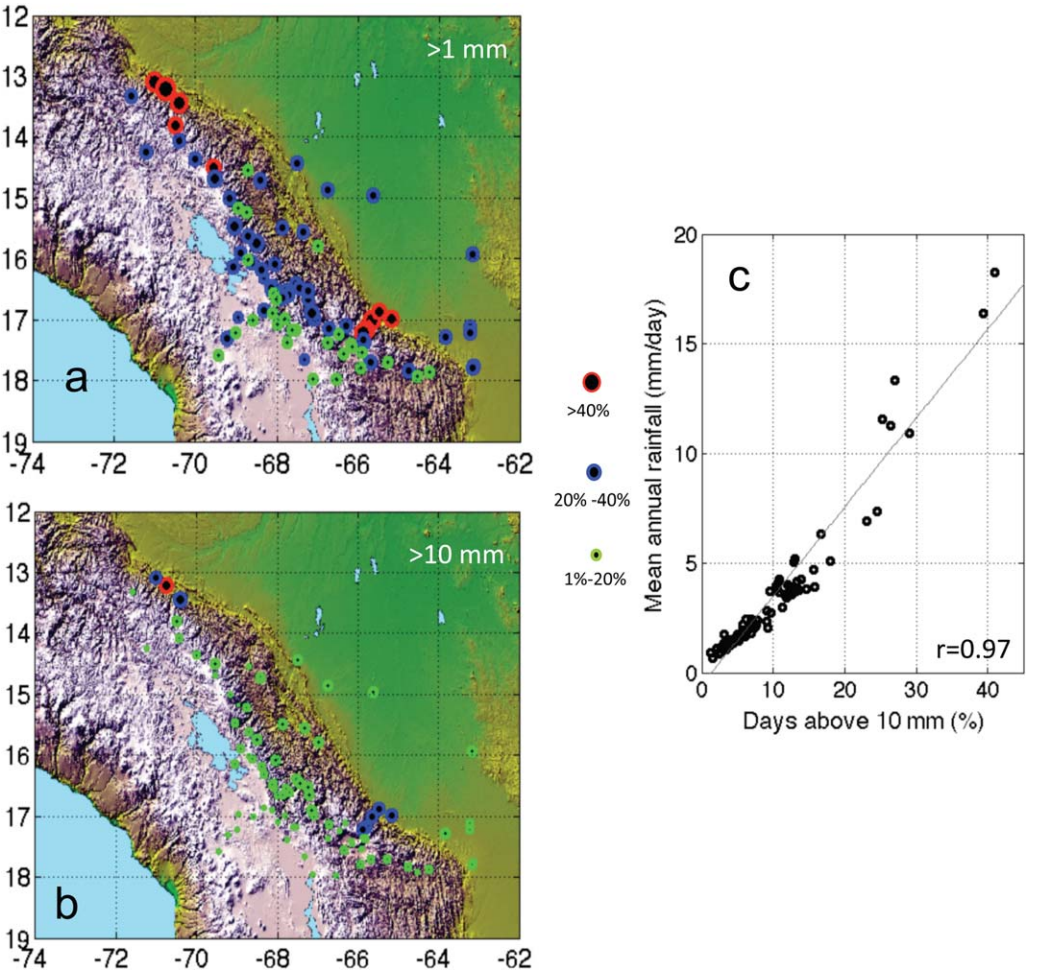

Figure 3. Percentage of days with rainfall above (a) 1 mm/d and (b) 20 mm/d in the 1970–2005 period. (c) Relationship between the percentage of days with rainfall above 10 mm/d and mean annual rainfall (mm/d) at the 95 meteorological stations.

variability in annual rainfall. Very rainy days (i.e., with more than 10 mm rainfall) represent 20%–40% of the days in the hotspot regions (Figure 3b). The highest percentages are recorded at the Quincemil and San Gabán meteorological stations (40%), in Pilcopata and in the Bolivian hotspot (around 30%). These values drop to 10%–15% in the Bolivian lowlands and to 2% in the Altiplano. The frequency of very rainy days thus explains much more annual rainfall variance (94%) than rainy days (Figure 3c). The simple linear model in equation (1) represents this relationship:

$$P_{An} = 0.405 \times P_{10} - 0.536 \quad (1)$$

where P_{An} is mean annual precipitation (mm/d) and P_{10} is the percentage of days with rainfall > 10 mm ($r = 0.97$, $N = 95$, $p \leq 0.001$).

4. Seasonal Cycle and Extreme Rainfall Events

In the Altiplano and the southern Andes, dry conditions prevail from May to September, while 20–100 mm rainfall/month are reported over the Bolivian lowlands. In the hotspot regions, monthly rainfall reaches 600 mm in Cristal Mayu and 850 mm in San Gabán during austral summer (Figure 4). To analyze the contribution of extreme rainy days to total rainfall, we identified days with rainfall above the 90th percentile, which are defined as extreme rainfall events. Thresholds were identified for each meteorological station and for each month. The red lines in Figure 4 show the accumulated monthly rainfall that corresponds to days with extreme rainfall events. The contribution of extreme rainfall events remains relatively constant throughout the

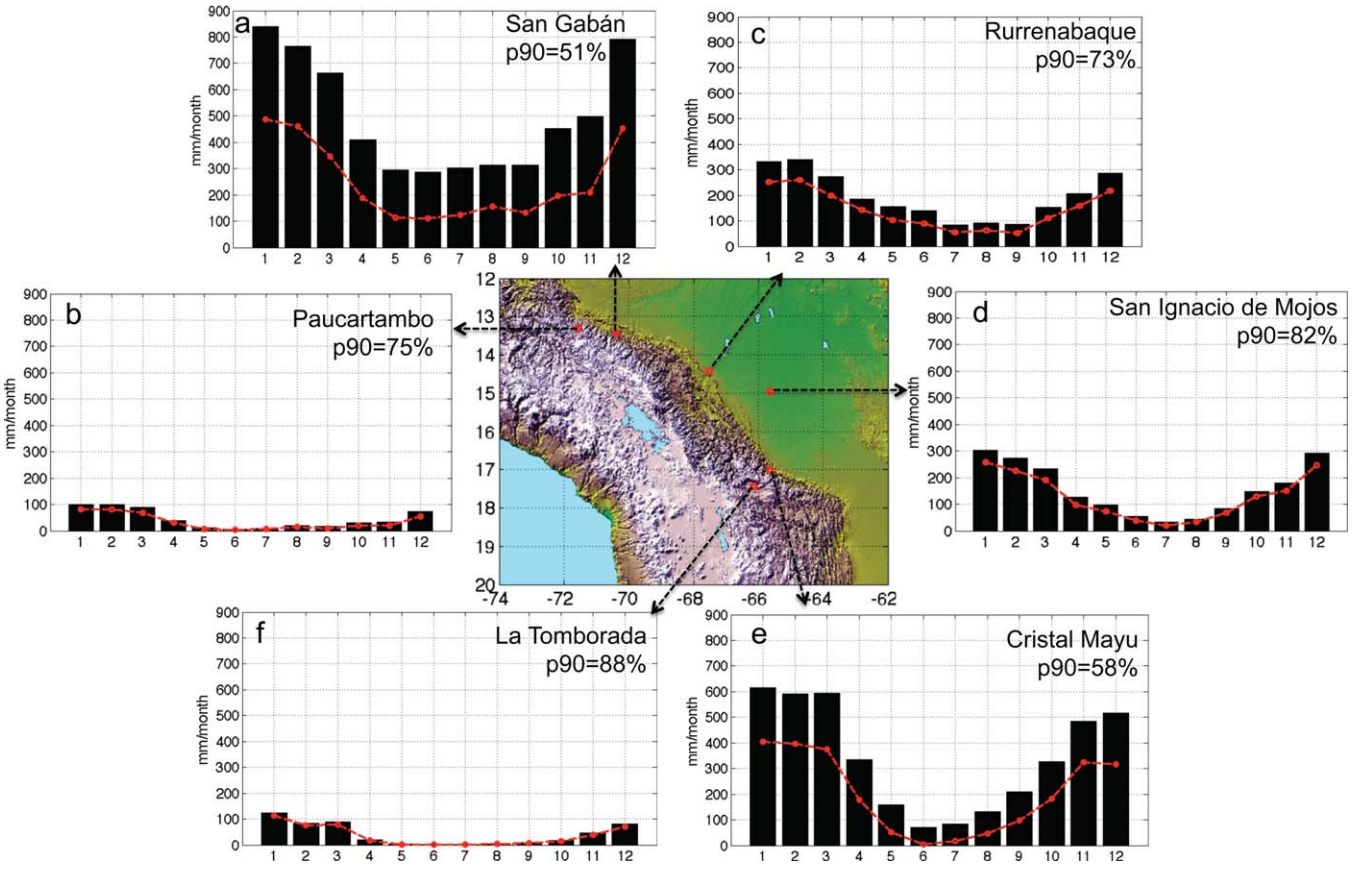

Figure 4. Mean annual rainfall cycle (1975–2005) for (a) San Gabán, (b) Paucartambo, (c) Rurrenabaque, (d) San Ignacio de Mojos, (e) Cristal Mayu, and (f) La Tomborada. Red lines represent monthly rainfall contributed by the rainiest days (days with rainfall above the 90th percentile). The percentage contribution of the rainiest days to total annual rainfall is indicated in each plot (p90).

year, corresponding to 70%–80% of total rainfall in the Amazon and eastern Andes but higher in the highlands (e.g., 88% at La Tomborada meteorological station; Figure 4f). However, the contribution of very rainy days to total rainfall is significantly lower (around a half total rainfall) in the hotspot regions, and extreme rainfall events contribute 51% and 58% to total rainfall at San Gabán and Chipiriri stations, respectively.

Figures 5 and 6 provide details about the seasonal cycle in the hotspot regions using TRMM 2A25 rainfall data and 850 hPa wind data originating from high-resolution ERA-interim re-analysis. Figures 5b and 5c, and 6b and 6c give rotated spatial coordinates to provide a 3-D view of the low-level atmospheric circulation from the Amazon to the Andes. As is true for meteorological stations, estimated rainfall in the northern hotspot is higher than in the southern one, and TRMM data reveals that the northern hotspot also extends over a larger area in both winter and summer than the southern hotspot (Figures 5a and 6a). The direction of the low-level winds over these regions may partly explain these differences. Figure 7 shows the angle between the direction of the 850 hPa wind and the dominant axis of the Andes in the DJF and JJA seasons near the hotspots. An angle of 90° (0°) indicates that the winds are approximately perpendicular (parallel) to the Andes. The axis of the Andes is given for each region (green line in Figure 7) and follows the main direction of the 1000 masl contour (black line in Figure 7). In the northern hotspot, low-level winds during summer are almost perpendicular to the topography over a large area (Figure 7a). This wind pattern is consistent with strong convection forced by the eastern foothills of the mountains, and up to 3000 mm rain falls during the DJF season (Figures 5a and 5b). In contrast, in the southern hotspot, the direction of the low-level wind is almost perpendicular up to only 50 km from the mountains, and it is predominantly parallel to the northwest-southeast range in the lowlands, which are located further away. Figure 7b also shows that the low-level wind becomes perpendicular to the mountains south of Chipiriri and Cristal Mayu meteorological stations, in the maximum rainfall region (2500 mm in DJF) estimated by TRMM 2A25 (Figures 5a and 5c).

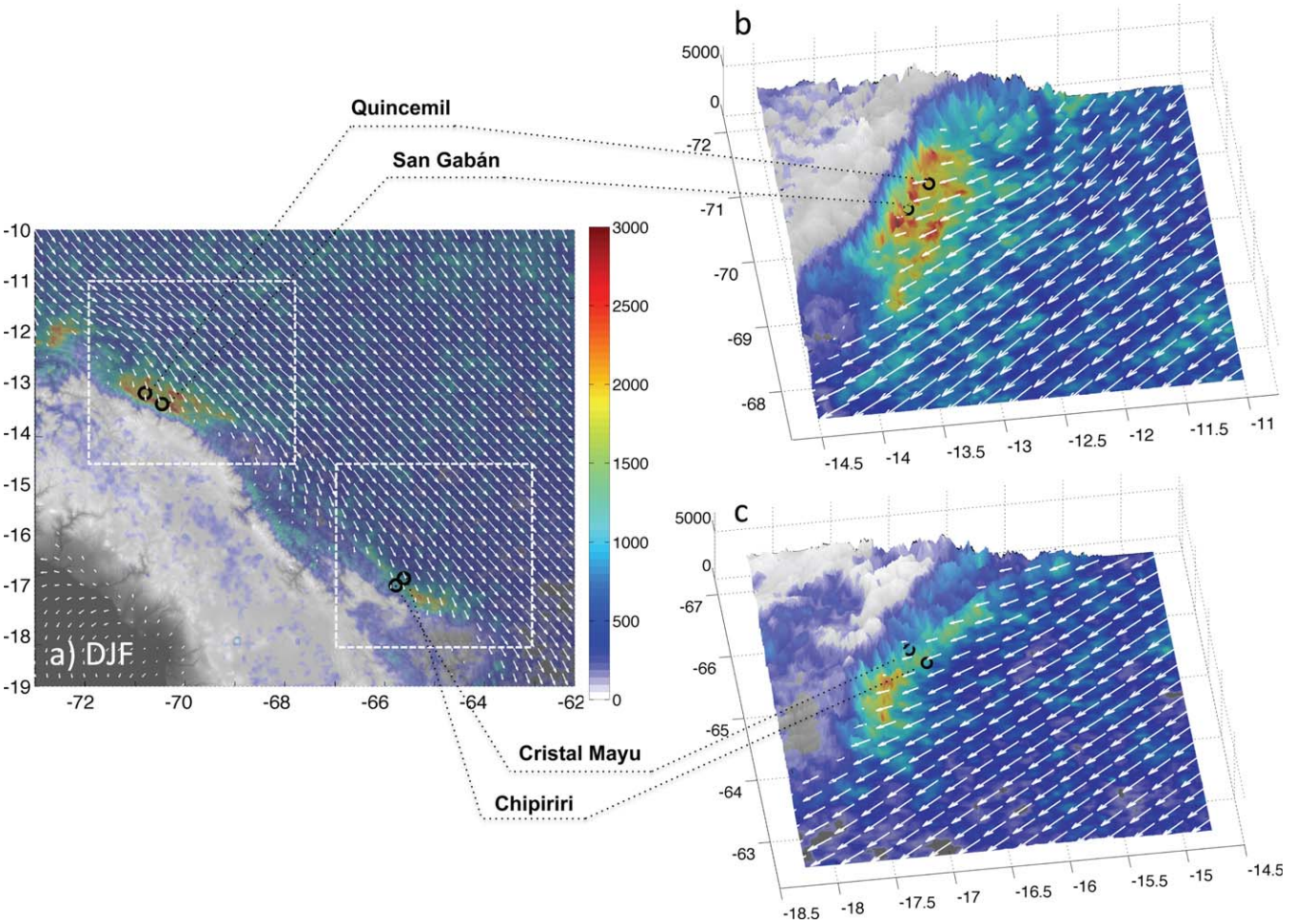

Figure 5. (a) Mean December to February (DJF) 850 hPa total wind from ERA-Interim (white vectors, m/s, 1998–2012) and accumulated rainfall (colors, mm, 1998–2012) estimated using TRMM PR 2A25 in the region of the Peruvian and Bolivian hotspots. Only values higher than 200 mm are plotted. Topography is derived from SRTM at 1 km resolution. (b) and (c) give a 3-D view of rainfall and 850 hPa wind in the Peruvian and Bolivian hotspots, respectively. Regions corresponding to Figures 5b and 5c are indicated with a white box in (a). In Figures 5b and 5c, TRMM data was resampled at the SRTM resolution (1 km). The locations of San Gabán, Quincemil, Chipiriri, and Cristal Mayu meteorological stations are indicated.

During austral winter, rainfall is particularly strong in the Peruvian hotspot, with up to 1000 mm during the JJA season, while it is less in the Bolivian hotspot or in the Amazon lowlands. Around 300 mm/month is recorded by the Quincemil and San Gabán meteorological stations from May to September (Figure 4a). The low-level wind shows that in the Peruvian hotspot, the wind still includes a strong component perpendicular to the eastern foothill of the Andes (Figure 7c), especially to the north of Quincemil, where a rainfall maximum is estimated by TRMM in winter (Figures 6a and 6b). In the Bolivian hotspot, the northwest-southeast wind, parallel to the mountain range, is intense, probably linked to the reinforcement by the South Atlantic anticyclone (Figures 6a and 6c). This circulation produces a wind component almost parallel to the Andes component (Figure 7d), which may explain the reduced convection over the Chipiriri and Cristal Mayu meteorological stations during the JJA season. However, south of Chipiriri and Cristal Mayu stations, the low-level wind includes a strong component perpendicular to the Andes, corresponding to a slight regional rainfall maximum over the Bolivian hotspot (Figures 7d and 6c).

Next, to provide more details about rainfall in the hotspot regions, we computed a rainfall index by averaging daily rainfall recorded at the Quincemil and San Gabán meteorological stations. This allowed us to preserve the continuity of the time series as well as to smooth part of the small-scale variability, thereby providing rainfall variability that is more representative of the synoptic scale. This procedure is valid in the Peruvian hotspot because rainfall in both stations, located at similar altitudes (about 700 masl, Figure 2b), is significantly correlated at the intraseasonal time scale ($r = 0.50$, $p \leq 0.001$). In contrast, in the Bolivian hotspot, the Chipiriri, and

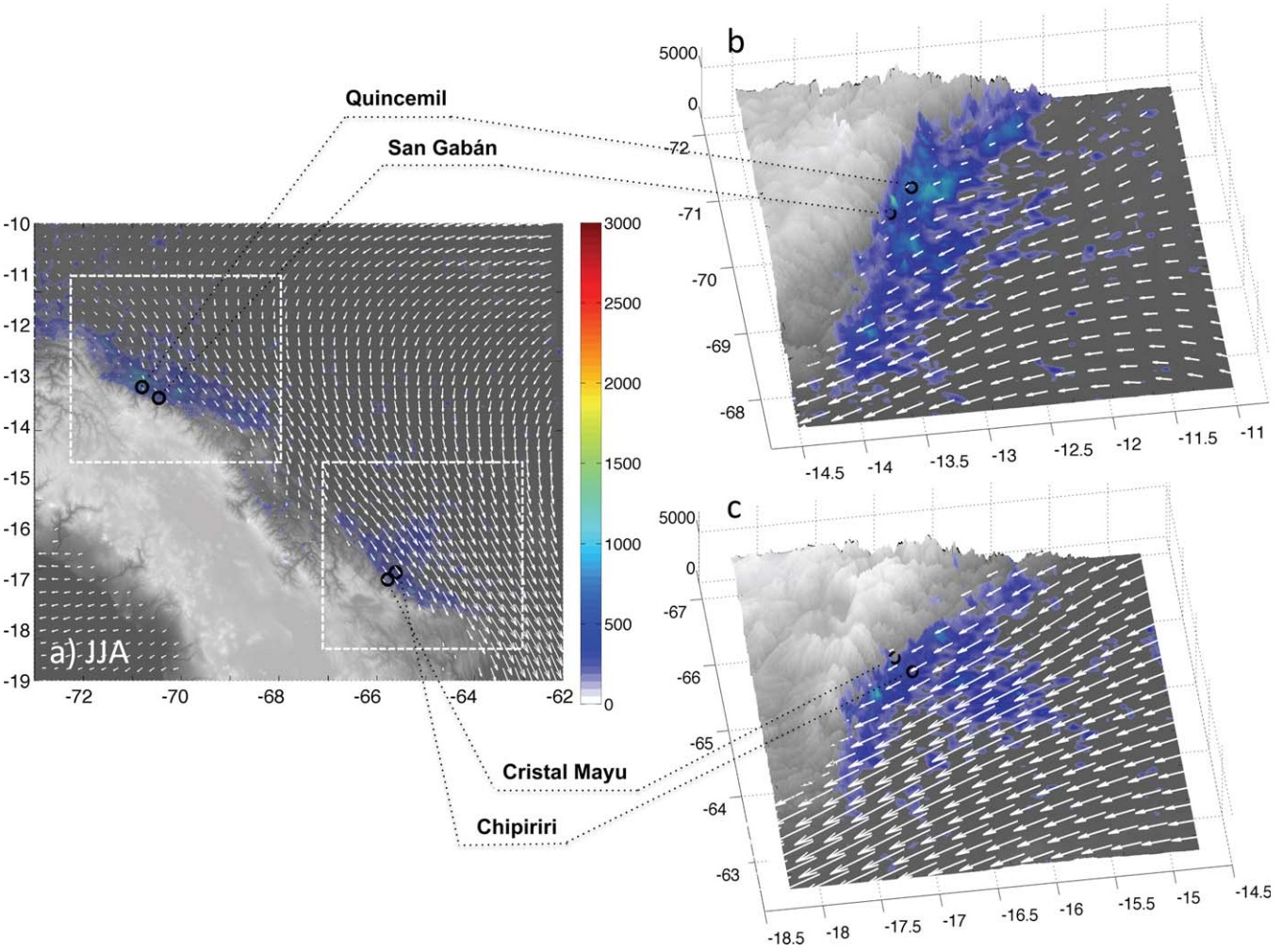

Figure 6. As in Figure 5, but for the June July August (JJA) season.

Cristal Mayu stations, which are located close to one another, are not significantly correlated. This may be due to the altitudinal difference between the stations (one at 411 and the other at 810 masl; Figure 2c).

The accumulated probability density function of the Peruvian hotspot index values was computed for the 1975–2005 period. Extreme rainfall values, delimited by the 90th percentile, increase from 30 mm/d in JJA to 60 mm/d in DJF (Figure 8a). Considering the latitudinal position of the Peruvian hotspot (13.3°S), it is remarkable to find rainfall higher than 30 mm on 10% of the winter days (i.e., ∼10 days for each JJA season). In this region, the number of days without rainfall ranges from 38% in JJA to 18% in DJF season. Moreover, sequences of at least three consecutive dry days are observed in 10% of the JJA days (i.e., three cases for each JJA), whereas such sequences are exceptionally rare in the DJF season (∼3%; Figures 8b and 8c). Given that exceptional rainfall is observed during the austral winter in the Peruvian hotspot, in the following section, we analyze the atmospheric circulation related to extreme events over this region taking into account two cases: (i) days with rainfall higher than the 90th percentile (30 mm/day, 10% of the days) and (ii) dry events characterized by at least three consecutives dry days (10% of the days).

5. Extreme Rainfall Events and Their Relationship With Atmospheric Circulation During Austral Winter

In this section, we analyze the relationship between extreme rainfall events in the hotspot regions and the regional atmospheric circulation. To this end, composites of 850 hPa winds and geopotential height from

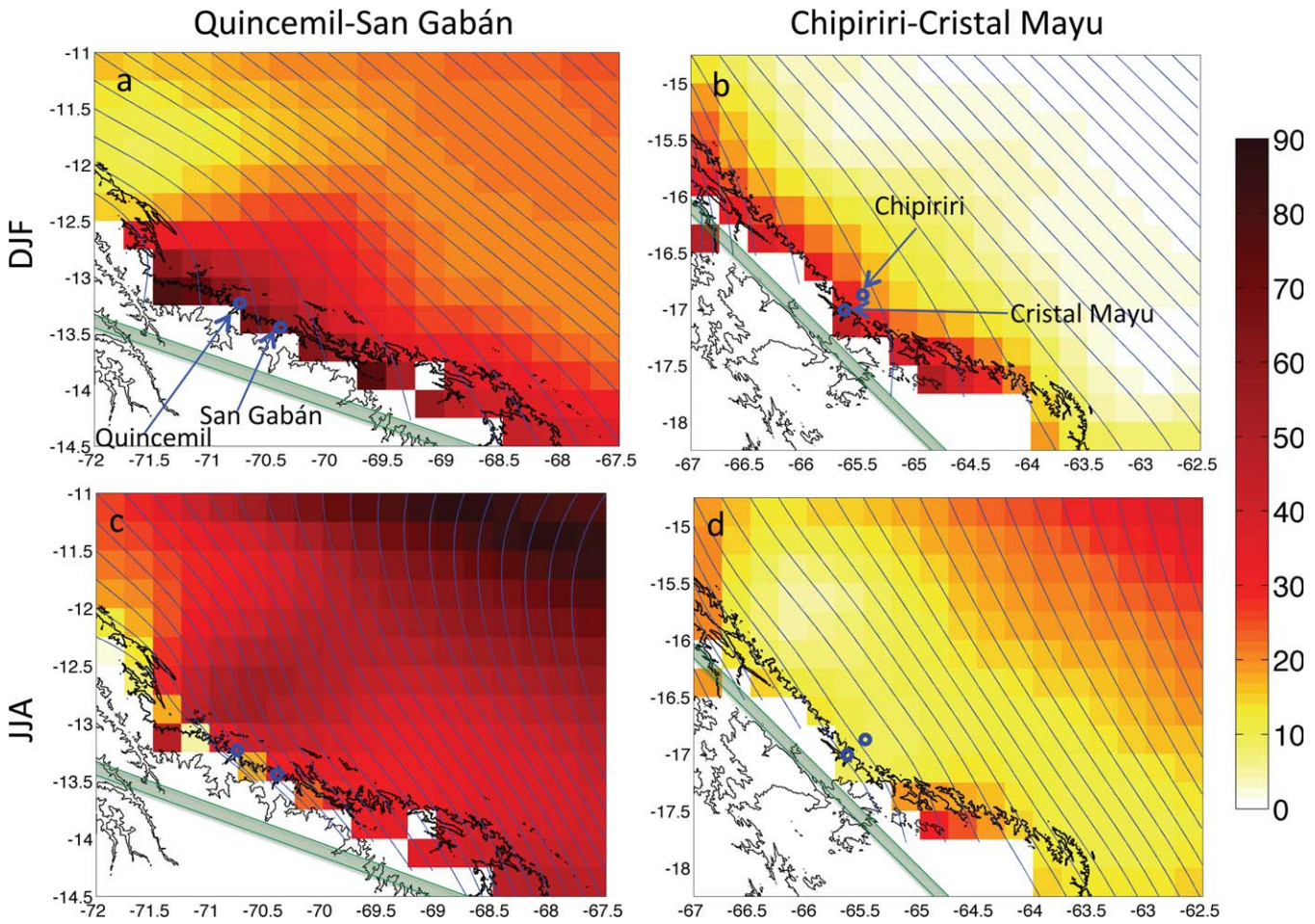

Figure 7. Angle between the total 850 hPa wind and the Andes axis for the DJF (a) and (b) and JJA (c) and (d) seasons. The axis of the Andes (thick green line) is defined following the main direction of the 1000 masl contour (black line) for each region. The stream function from 850 hPa winds is in blue. Total wind was computed using the ERA-Interim (1998–2012) data set on a 0.25° × 0.25° grid resolution.

ERA-40 reanalysis were computed during extreme dry and wet events in the Peruvian hotspot during austral winter.

5.1. Extreme Dry Events in the Peruvian Hotspot

Periods with at least three consecutive dry days in the Peruvian hotspot are defined as extreme dry events. In the composite analysis, each day is noted "D*n*," where *n* is the number of days relative to the first of these dry days, which is noted D0 (Figure 9d). On average, we observe three extreme dry episodes per year (10% of JJA days, Figure 8b). Composite analysis shows that in the three preceding days (D–3 to D–1), midlatitude positive geopotential anomalies (centered at 40°S) intensify and move eastward (Figures 9a–9c). These geopotential anomalies are stronger over the continent at D–1, where anticyclogenesis is well developed, and produces southern wind anomalies over the southern Amazon (Figure 9c). At the beginning of the dry event (D0), southern wind anomalies reach the equatorial Amazon region. Southerly wind regimes extending from the La Plata basin to the Peruvian Amazon predominate on the dry days (D0 to D+2), in association with the eastward migration of midlatitude positive geopotential anomalies (Figures 9d–9f). Southerly wind regimes produce a deficit of humidity advection over the Peruvian Amazon, which explains the absence of precipitation from D0 to D+2. Changes in atmospheric circulation from D-3 to D+2 have already been described in terms of large-scale circulation patterns (CP) [*Espinoza et al*., 2012, 2013]. Changes from D-3 to D+2 correspond to a well-organized transition from CP1 to CP6 (defined in *Espinoza et al*. [2013]). In addition, extreme dry events (D0 to D+2) correspond to cold surges reaching the Peruvian Amazon region (CP4 to CP6).

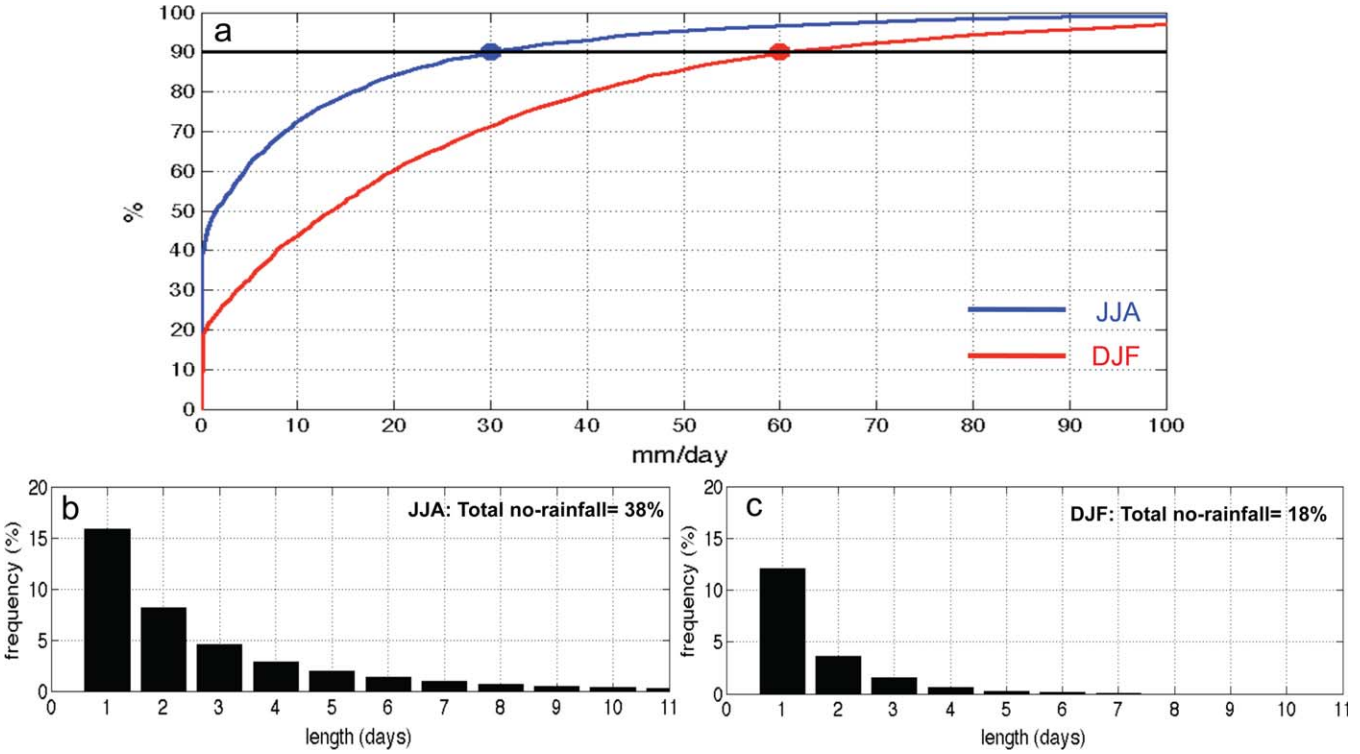

Figure 8. (a) Accumulated probability density function for Quincemil-San Gabán daily rainfall index (1975–2005 period). Blue and red lines represent the JJA and DJF seasons, respectively. (b) and (c) show the frequency of dry sequences (in days) during 1–11 consecutive days in the JJA and DJF seasons, respectively. The total number of dry days during each season is indicated.

5.2. Wet Extreme Events in the Peruvian Hotspot

In this case, D0 corresponds to days with rainfall above the 90th percentile (30 mm) in the Peruvian hotspot. Composite analysis show that from D–3 to D–1, midlatitude negative geopotential anomalies predominate over the continent. These low geopotential conditions enhance northerly wind anomalies to the east of the tropical Andes, from the Amazon region to southeastern South America (Figures 9g–9i). At D0, negative geopotential anomalies move eastward and southerly wind incursions are observed in Argentina east of the Andes, resulting in the convergence of winds over the northern La Plata basin and in the southern Amazon basin (Figure 9j). In addition, D0 is characterized by a strong northerly wind regime from the Atlantic Ocean and northern Amazon. Thus, the intense humidity advection from the north and the convergence enhanced by southern winds may explain the extreme rainfall in the Peruvian hotspot on D0. Changes between D-3 and D+2 (Figures 9g–9l) resemble the CP transition from CP7 to CP3 described by *Espinoza et al.* [2013]. Indeed, these CPs are characterized by a northerly wind regime and warmer conditions over the Peruvian Amazon [see *Espinoza et al.*, 2013, Figure 5].

To summarize, composites of the atmospheric circulation during extreme dry and wet events in the Peruvian hotspot reveal a well-defined relationship between rainfall events and the circulation of large-scale winds. In particular, extreme rainfall events are clearly linked with southerly (dry periods) and northerly (wet periods) wind regimes. In the following paragraph, we use the cross-equatorial wind index defined by *Wang and Fu* [2002] to further explore the effects of wind regimes on extreme rainfall events in the Peruvian hotspot.

5.3. Cross-Equatorial Winds and Rainfall in the Southern Tropical Andes

To define northerly and southerly wind regimes over the Amazon region, we computed the index based on the cross-equatorial wind proposed by *Wang and Fu* [2002]. To this end, we used ERA-40 850 hPa meridional wind anomalies averaged over the 5°N–5°S, 65°W–75°W region. This index is attractive because, being a remote regional index, it may help forecast rainfall in the Peruvian hotspot. We also compared our results with winds recorded at Iquitos meteorological station, which is situated in the region where the cross-

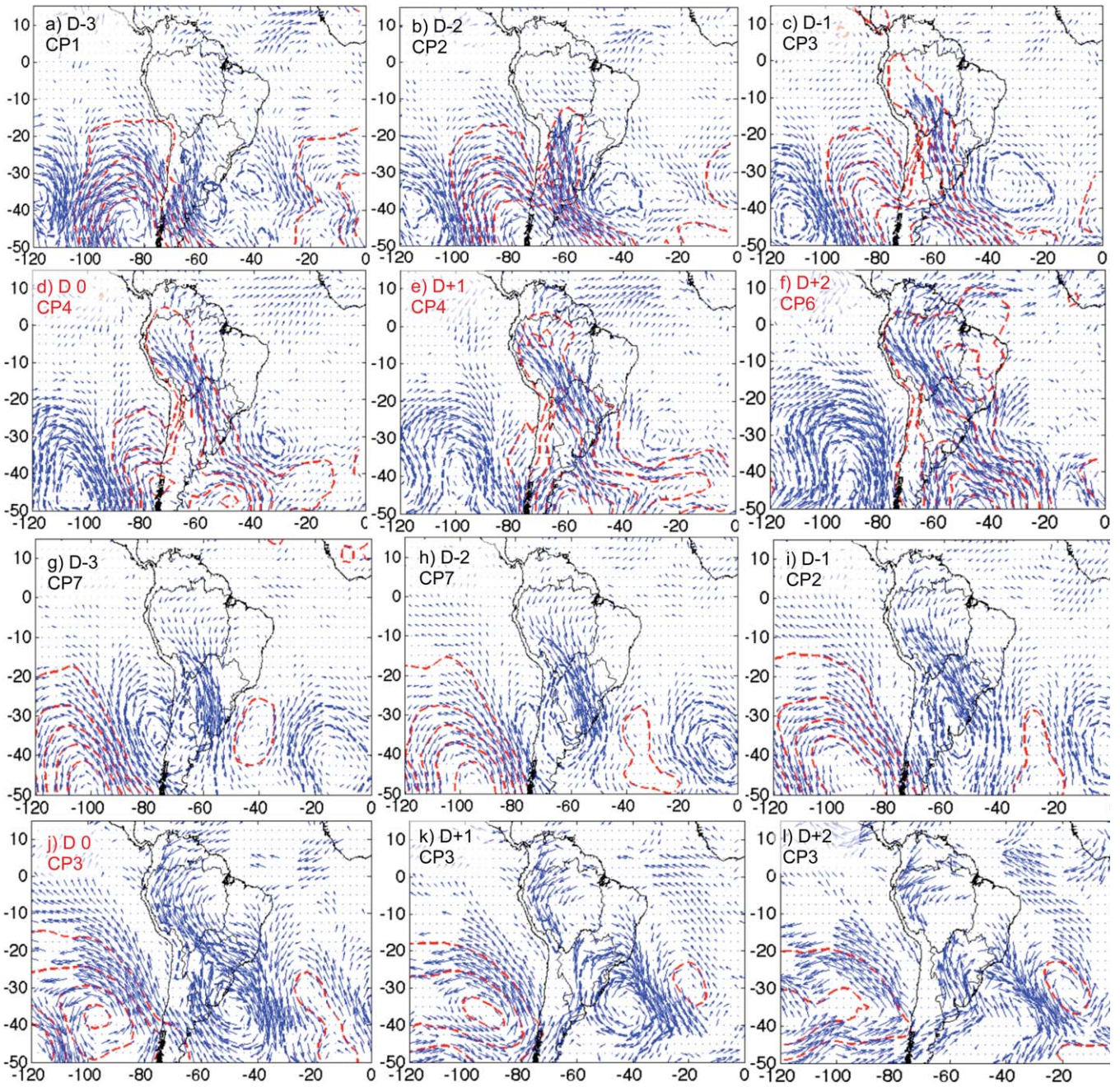

Figure 9. Composites of wind (vectors, m/s) and geopotential height (contours, m) anomalies at 850 hPa from D–3 to D+2 for (a)–(f) dry events and (g)–(l) wet events. Only wind differences higher than 0.2 m/s are plotted. Circulation patterns associated with each day are indicated; the patterns are defined in *Espinoza et al*. [2013].

equatorial winds were computed (Figure 10a). A southerly (northerly) regime is characterized by days with a positive (negative) 850 hPa meridional wind anomaly plus (minus) a standard deviation. Using this criterion, ∼15% of JJA days were characterized by a northerly regime and ∼15% by a southerly regime.

We evaluated the accumulated probability of rainfall distribution in the Peruvian hotspot using both southerly (V+) and northerly regimes (V-) computed from ERA-40. During northerly regimes, 30% of dry days occur, while the 90th percentile reaches 44 mm/d (bold blue line in Figure 10a). In contrast, during southerly regimes, the probability of dry days doubles (60%) and precipitation >10 mm/d rarely occurs (bold red line in Figure 10a). These results show that intense rainfall in the Peruvian hotspot ($>$30 mm/day) occurs predominantly during northerly regimes. Moreover, using wind regimes similarly computed from data

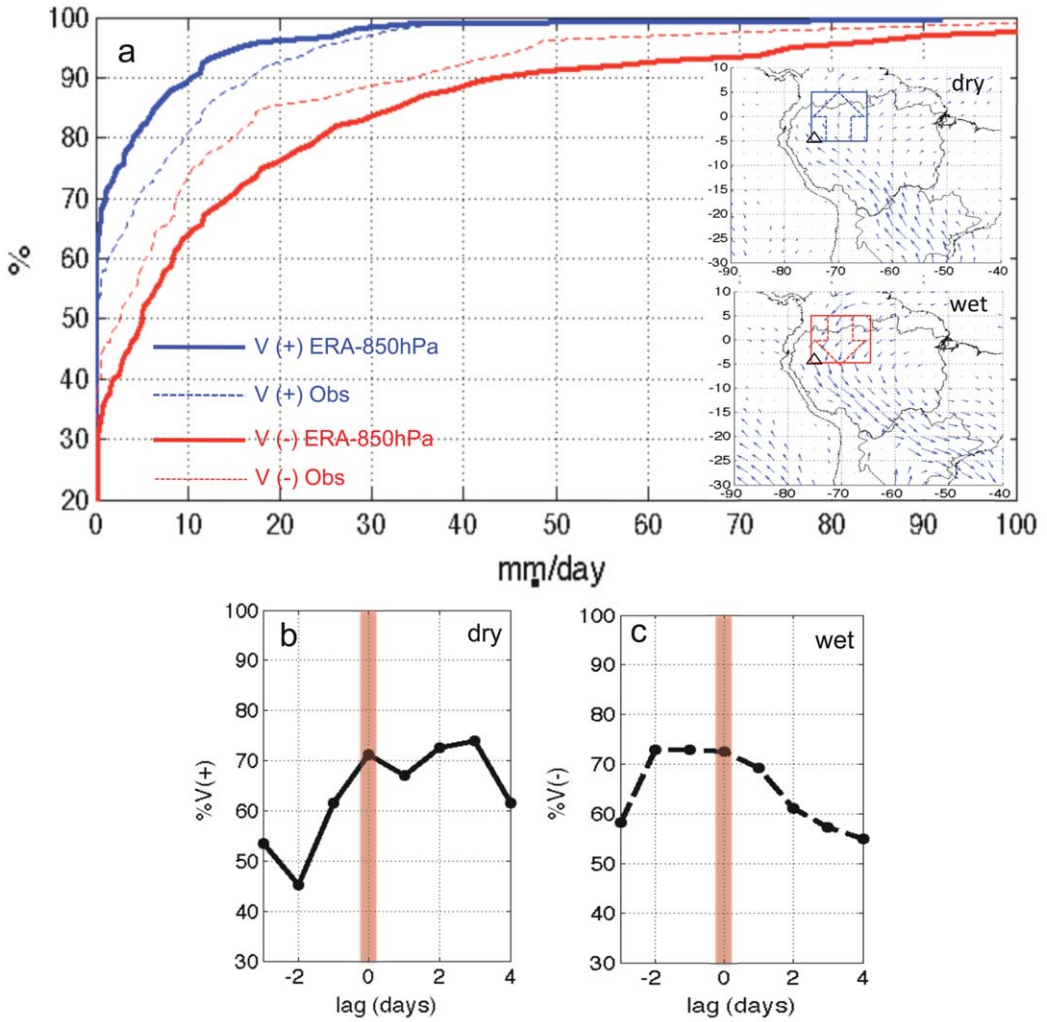

Figure 10. (a) Accumulated probability density function of Quincemil-San Gabán rainfall index during the JJA season, during a southerly regime (V+, blue line) and a northerly regime (V-, red line). Wind regimes were computed using information at 850 hPa from ERA-40 (solid line) and from Iquitos meteorological station (dashed line). The town of Iquitos and the region in which the cross-equatorial winds were computed are indicated in the right plots. (b) Composite analysis of the percentage of days corresponding to southerly regimes during dry events from D-3 to D4. (c) Composite analysis of the percentage of days corresponding to northerly regimes during wet events from D-3 to D4.

recorded at the Iquitos meteorological station, we observe that differences in rainfall probability in the Peruvian hotspot are almost the same, although not as acute (dashed lines in Figure 10a). The probability of dry days increases from 37% to 52% during northerly and southerly regimes, respectively, while intense rainfall ($>$ 30 mm/day) only occurs during northerly regimes, as recorded at Iquitos meteorological station. In conclusion, major differences in rainfall probability during both regimes call for further/future investigations using this wind index to forecast rainfall in the Peruvian hotspot.

Considering the extreme dry and wet events defined in section 5.2 and Figure 8, we conclude that extreme dry days (three consecutive dry days) are characterized by a southerly regime in around 70% of the cases, while 72% of extreme wet days ($>$30 mm/day) are characterized by a northerly regime (Figures 10b and 10c). This analysis also reveals that extreme dry days are characterized by a progressive change in the wind regime from D-2 (when a northerly regime predominates) to D 0, when a southerly regime predominates and that this situation persists during the four following days (Figure 10b). In contrast, extreme wet days are linked to the occurrence of a northerly regime starting at D-2 that persists during the two following days (Figure 10c). Figures 9g–9j, which are characterized by northerly regimes, show that wind convergence in the southern Amazon is necessary to produce extreme wet events (Figure 9j).

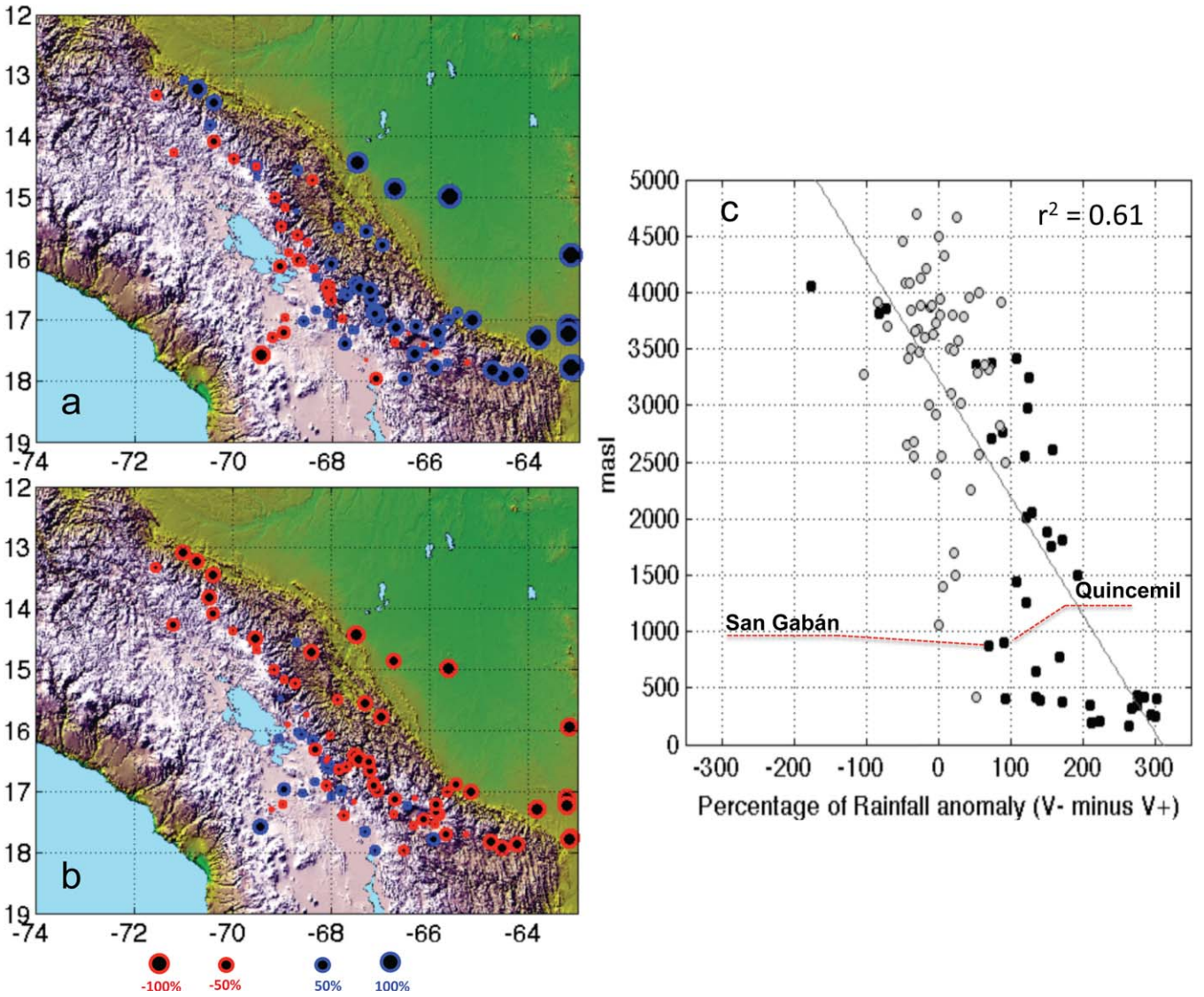

Figure 11. JJA rainfall anomalies (1975–2001) during days characterized by (a) a northerly regime (V-) and (b) a southerly regimes (V+). Anomalies are normalized by the mean JJA rainfall recorded at each meteorological station. Northerly and southerly regimes were computed using 850 hPa wind anomalies from ERA-40. (c) Difference between rainfall anomalies during northerly and southerly regimes versus the altitude of each station. The linear regression is plotted. Black-filled circles indicate significant differences according to a t-test ($p < 0.05$).

We also evaluated the influence of the cross-equatorial winds considering the 95 meteorological stations distributed over the southern tropical Andes. In this case, rainfall anomalies were computed during the northerly and southerly regimes recorded at each station (Figure 11). During northerly regimes, positive rainfall anomalies predominate over the Bolivian lowlands (up to 200%) and on the eastern flank of the Andes (50%–100%). Over the mountains and the Altiplano (regions above 3500 masl), weak negative rainfall anomalies (around −20%) occur during a northerly regime (Figure 11a). In addition, during southerly regimes, rainfall anomalies are negative in the Amazon (−90%) and east of the Andes (−70%) and near to zero or slightly positive (generally <20%) over the Altiplano (Figure 11b). These results suggest that the influence of a cross-equatorial flux at 850 hPa on rainfall has a spatial pattern, contrasting the east of the Andes (clear influence) and highlands/Altiplano (weak or no influence). Indeed, previous studies have already shown the influence of eastern winds at high levels (e.g., 200 hPa) in modulating rainfall in the highlands/Altiplano region [e.g., *Garreaud et al.*, 2003; *Minvielle and Garreaud*, 2011].

To quantify the influence of cross-equatorial winds on rainfall, we computed an index based on rainfall anomalies during northerly regimes minus rainfall anomalies during southerly regimes, for each

meteorological station. The influence of cross-equatorial winds appears to be clearly linked with altitude ($r^2=0.61$; Figure 11c). Figure 11c shows the strong influence of cross-equatorial winds at meteorological stations located below 2000 masl, where rainfall anomalies during northerly regimes are generally 100% higher than during southerly regimes. This difference in rainfall anomalies is significant (according to a t-test, $p < 0.05$) at 84% of the rainfall stations located below 2000 masl. At stations located between 2500 and 3500 masl, a significant influence of cross-equatorial winds is observed at 30% of the stations. Nevertheless, above 3500 masl, rainfall anomalies between northerly and southerly regimes predominate from −50% to 50% and only three stations (at ∼4,000 masl) are significantly influenced by cross-equatorial winds (Figure 11c). However, in this case, the influence of cross-equatorial winds is opposite, albeit weak, to that observed in the lowlands. At stations above 3500 masl, characterized by very dry conditions during JJA, some rainy days occur during southerly regimes, probably associated with an uplift of humid air masses from the lowlands forced by cold air masses during southerly cold surge episodes. Indeed, cold surges (also called *friajes* or *surazos* in Peru and Bolivia) are particularly intense during austral winter [e.g., *Garreaud*, 2000; *Lupo et al*., 2001; *Espinoza et al*., 2013] and may even produce snowfall events in the tropical Andes [*Vuille and Ammann*, 1997]. These results suggest that cross-equatorial winds are useful indicators of the circulation anomalies that modulate the intraseasonal rainfall variability over the lowlands, while a gradual decrease in this influence is observed east of the Andes in relation to altitude. The windward or leeward locations of the rainfall stations may partly explain the remaining variance (not explained by altitude, 39%), particularly above 2500 masl.

6. Summary and Concluding Remarks

The exceptional spatial variability of rainfall in the Eastern tropical Andes is evidenced and discussed in this paper using observed daily rainfall from 95 meteorological stations located in Bolivia and Peru. Of particular interest are the extreme rainfall regions (hotspots), which correspond to the most biologically rich region of the world. Hotspot regions are identified at low elevations in the Andes foothills (400–700 masl) and in windward conditions, which is the case of Quincemil-San Gabán (Peru) and in Chipiriri-Cristal Mayu (Bolivia), where more than 4000 mm rain fall per year. Orographic effects and exposure to easterly winds produce a strong rainfall gradient that can reach 190 mm/km, even between two stations located at similar elevations (3000 masl). Rainfall features were also examined using TRMM-PR 2A25. We found that this product underestimates rainfall by 35% in the hotspot regions (Quincemil, San Gabán, Chipiriri stations), and by even more (up to 80%) in the highlands. These results suggest that satellite information needs to be calibrated to render their representation of rainfall more accurate.

In the hotspot regions, abundant rainfall occurs all year round; for instance, in the Peruvian hotspot, the 90th percentile of rainfall distribution increases from 30 to 60 mm/d, while dry days decrease from 38% in the dry season (JJA) to 18% in the wet (DJF) season. The contribution of extreme rainfall events to the total monthly rainfall remains relatively constant throughout the year. It is > 70% in the Amazon, the eastern Andes and the Altiplano. However, in the hotspot regions, the contribution of very rainy days is considerably lower, approximately half total rainfall. Rainfall recorded at San Gabán and Quincemil meteorological stations (Peruvian hotspot) is more intense, particularly in winter, than at Chipiriri and Cristal Mayu stations (Bolivian hotspot). Low-level wind circulation partly explains these seasonal rainfall differences. In the northern hotspot, low-level winds blow almost perpendicular to the eastern foothills of the Andes all year round, which can enhance local circulation and convection forced by the topography. In contrast, in the southern hotspot, northwest-southeast winds blow parallel to the Andes, and are more intense in austral winter, linked to the enhancement of the South Atlantic anticyclone.

By analyzing intraseasonal rainfall variability in JJA, we found that extreme rainy events over the eastern tropical Andes are clearly linked to large-scale atmospheric circulation. In particular, cross-equatorial wind variability in the low troposphere appears to play a key role in explaining the extreme wet and dry episodes in this region. During northerly wind regimes, positive rainfall anomalies predominate over the Bolivian Amazon (up to 200%) and on the eastern flank of the Andes (50% to 100%), while the anomalies are weak or negative over the high mountains and the Altiplano (around −20%). In contrast, during southerly regimes, rainfall anomalies are negative in the Amazon (−90%) and east of the Andes (−70%) and near to zero or slightly positive (generally <20%) over the Altiplano. In the Peruvian hotspot, extreme dry days

(three consecutive dry days) are characterized by a southerly regime in around 70% of the cases, while intense rainfall in the Peruvian hotspot (>30mm/d) occurs predominantly during northerly regimes. Our results show that cross-equatorial winds play an important role in modulating rainfall variability in the lowlands, while a gradual decrease in this influence is observed east of the Andes in relation to altitude and orography (location windward or leeward, particularly notable above 2000 masl). The influence of cross-equatorial winds is slight or nonexistent above 3500 masl.

Finally, these results provide a basis for future work, which will be of particular interest for managers of water resources, hydrological modeling, and for the scientific community involved in climate studies in Andean-Amazonian countries. Special efforts will be focused on (i) quantifying erosion dynamics in relation to extreme rainfall in the upper part of Madre de Dios, Beni, and Mamoré rivers, whose basins include the hotspot regions, and (ii) developing a high-resolution climate model to explore the atmospheric physics related to climate-orography interactions.

Acknowledgments

We wish to thank the following agencies/organizations for providing access to data: NASA for TRMM data (http://disc.sci.gsfc.nasa.gov/precipitation/documentation/TRMM_README), the European Centre for Medium-Range Weather Forecasts (ECMWF) for the ERA40 (http://data-portal.ecmwf.int/data/d/era40_daily), and the ERA-Interim (http://apps.ecmwf.int/datasets/data/interim_full_daily/) reanalysis, and SENAMHI from Bolivia and Peru for the historical rainfall observations (www.senamhi.gob.bo and www.senamhi.gob.pe, respectively). We also thank the PNICP-Peru for providing funds through the "contrato 397-PNICP-PIAP-2014" contract. The authors are grateful to the reviewers for their contribution to improve this paper and to Daphne Goodfellow for correcting accurately the manuscript.

References

Aceituno, P., and A. Montecinos (1993), Circulation anomalies associated with dry and wet periods in the South American Altiplano, in *Proceedings of the Fourth International Conference on Southern Hemisphere Meteorology, Hobart, Australia*, edited by Institut français d'études andines, IFEA, pp. 330–331, Am. Meteorol. Soc., Lima, Peru. [Available at http://www.ifeanet.org/publicaciones/detvol.php?codigo=183.]

Arraut, J. M., and P. Satyamurty (2009), Precipitation and water vapor transport in the Southern Hemisphere with emphasis on the South American region, *J. Appl. Meteorol. Climatol.*, *48*, 1902–1912.

Berbery, E. H., and V. R. Barros (2002), The hydrologic cycle of the La Plata basin in South America, *J. Hydrometeorol.*, *3*, 630–645.

Berri, G. J., and J. B. Inzunza (1993), The effect of the low-level jet on the poleward water vapour transport in the central region of South America, *Atmos. Environ.*, *27A*, 335–341.

Bookhagen, B., and M. R. Strecker (2008), Orographic barriers, high-resolution TRMM rainfall, and relief variations along the eastern Andes, *Geophys. Res. Lett.*, *35*, L06403, doi:10.1029/2007GL032011.

Buarque, D. C., R. T. Clarke, and C. A. B. Mendes (2010), Spatial correlation in precipitation trends in the Brazilian Amazon, *J. Geophys. Res.*, *115*, D12108, doi:10.1029/2009JD013329.

Byerle, L. A., and J. Peagle (2002), Description of the seasonal cycle of low-level flows flanking the Andes and their interannual variability, *Meteorológica*, *27*, 71–88.

Carvalho, L., C. Jones, and B. Liebmann (2002a), Extreme precipitation events in southeastern South America and large-scale convective patterns in the South Atlantic convergence zone, *J. Clim.*, *15*, 2377–2394.

Carvalho, L., C. Jones, and M. A. F. Silva Dias (2002b), Intraseasonal large-scale circulations and mesoscale convective activity in tropical South America during the TRMM-LBA campaign, *J. Geophys. Res.*, *107*(D20), 8042, doi:10.102/2001JD000745.

Chavez, S. (2013), Characterization of storms in the Mantaro Valley (Tropical Andes of Central Peru) using remote Sensing [in Spanish], Lic. in physics thesis, 114 pp., Pontificia Univ., Instituto Católica del Perú (IGP). [Available at: http://www.met.igp.gob.pe/publicaciones/2013/TesisSChavez.pdf.]

Condom, T., P. Rau, and J. C. Espinoza (2011), Correction of TRMM 3B43 monthly precipitation data over the mountainous areas of Peru during the period 1998–2007, *Hydrol. Processes*, *25*, 1924–1933. doi:10.1002/hyp.7949.

Dee, D., et al. (2011), The ERA interim reanalysis: Configuration and performance of the data assimilation system, *Q. J. R. Meteorol. Soc.*, *137*, 553–597, doi:10.1002/qj.828.

De Souza, E. B., and T. Ambrizzi (2006), Modulation of the intraseasonal rainfall over tropical Brazil by the Madden–Julian oscillation, *Int. J. Clim.*, *26*, 1759–1776.

El Comercio (2010), *Perú*, 8th ed. [Available at http://elcomercio.pe.]

Espinoza, J. C., J. Ronchail, J. L. Guyot, G. Cochonneau, N. Filizola, W. Lavado, E. de Oliveira, R. Pombosa, and P. Vauchel (2009), Spatio–temporal rainfall variability in the Amazon Basin Countries (Brazil, Peru, Bolivia, Colombia and Ecuador), *Int. J. Climatol.*, *29*, 1574–1594.

Espinoza, J. C., M. Lengaigne, J. Ronchail, and S. Janicot (2012), Large-scale circulation patterns and related rainfall in the Amazon basin: A neuronal networks approach, *Clim. Dyn.*, *38*, 121–140, doi:10.1007/s00382-011-1010-8.

Espinoza, J. C., J. Ronchail, F. Frappart, W. Lavado, W. Santini, and J. L. Guyot (2013), The major floods in the Amazonas River and tributaries (Western Amazon basin) during the 1970–2012 period: A focus on the 2012 flood, *J. Hydrometeorol.*, *14*, 1000–1008, doi:10.1175/JHM-D-12-0100.1.

Espinoza, J. C., J. A. Marengo, J. Ronchail, J. Molina, L. Noriega, and J. L. Guyot (2014), The extreme 2014 flood in south-western Amazon basin: The role of tropical-subtropical south Atlantic SST gradient, *Environ. Res. Lett.*, *9*, 124007, doi:10.1088/1748–9326/9/12/124007.

Falvey, M., and R. D. Garreaud (2005), Moisture variability over the South American Altiplano during the South American low level jet experiment (SALLJEX) observing season, *J. Geophy. Res.*, *110*, D22105, doi:10.1029/2005JD006152.

Figueroa, S. N., and C. A. Nobre (1990), Precipitation distribution over central and western tropical South America, *Climanalise*, *6*, 36–40.

Garreaud, R., M. Vuille, and A. Clement (2003), The climate of the Altiplano: Observed current conditions and mechanism of past changes, *Paleogeogr. Palaeoclimatol. Palaeoecol.*, *194*(3054), 1–18.

Garreaud, R. D. (2000), Cold air incursions over Subtropical South America: Mean structure and dynamics, *Mon. Weather Rev.*, *128*, 2544–2559.

Garreaud, R. D. (2001), Subtropical cold surges: Regional aspects and global distribution, *Int. J. Climatol.*, *21*(10), 1181–1197, doi:10.1002/joc.687.

Getirana, A. C. V., J. C. Espinoza, J. Ronchail, and O. C. Rotunno Filho (2011), Assessment of different precipitation datasets and their impacts on the water balance of the Negro River basin, *J. Hydrol.*, *404*, 304–322. doi:10.1016/j.jhydrol.2011.04.037.

Grimm, A. M., and R. G. Tedeschi (2009), ENSO and extreme rainfall events in South America, *J. Clim.*, *22*, 1589–1609.

Hijmans, R. J., S. E. Cameron, J. L. Parra, P. G. Jones, and A. Jarvis (2005), Very high resolution interpolated climate surfaces for global land areas. *Intern. J. Clim.*, *25*, 1965–1978, doi:10.1002/joc.1276.

Jones, C., and L. M. V. Carvalho (2002), Active and break phases in the South American Monsoon system, *J. Clim.*, *15*, 905–914.
Killeen, T. J., M. Douglas, T. Consiglio, P. M. Jørgensen, and J. Mejia (2007), Dry spots and wet spots in the Andean hotspot, *J. Biogeogr.*, *34*(8), 1357–1373, doi:10.1111/j.1365–2699.2006.01682.x.
Kodama, Y. (1992), Large–scale common features of subtropical precipitation zones (the baiu frontal zona, the SPCZ and the SACZ). Part I: Characteristic of subtropical frontal zones, *J. Meteorol. Soc. Jpn.*, *70*, 813–836.
Lavado, W. S., E. Silvestre, and W. Pulache (2010), Tendencias en los extremos de lluvias cerca a la ciudad del Cusco y su relación con las inundaciones de enero del 2010, *Rev. Peruana Geo-Atmos.*, *2*, 89–98.
Lenters, J., and K. H. Cook(1995), Comments on "on the influence of the Andes on the general circulation of the Southern hemisphere", *J. Clim.*, *8*, 2113–2115.
Liebmann, B., G. N. Kiladis, J. A. Marengo, T. Ambrizzi, and J. D. Glick (1999), Submonthly convective variability over South America and the South Atlantic convergence zone, *J. Clim.*, *12*, 1877–1891.
Liebmann, B., G. N. Kiladis, C. Vera, C. Saulo, and L. Carvalho (2004), Subseasonal variations of rainfall in South America in the vicinity of the low-level jet east of the Andes and comparison to those in the South Atlantic convergence zone, *J. Clim.*, *17*, 3829–3842.
Lowman, L. E. L., and A. P. Barros (2014), Investigating links between climate and orography in the central Andes: Coupling erosion and precipitation using a physical-statistical model, *J. Geophys. Res. Earth Surf.*, *119*, 1322–1353, doi:10.1002/2013JF002940.
Lupo, A. R., J. J. Nocera, L. F. Bosart, E. G. Hoffman, and D. J. Knight (2001), South American cold surges: Types, composites, and case studies, *Mon. Weather Rev.*, *129*(5), 1021–1041.
Marengo, J. A., and C. A. Nobre (2001), General characteristics and variability of climate in the Amazon Basin and its links to the global climate system, edited by M. E. McClain, R. L. Victoria, and J. E. Richey, pp., 17–41, The Biogeochemistry of the Amazon Basin, Oxford Univ. Press, Oxford, U. K.
Marengo, J. A., W. R. Soares, C. Saulo, and M. Nicolini (2004), Climatology of the low level jet east of the Andes as derived from the NCEP-NCAR reanalysis. Characteristics and temporal variability, *J. Clim.*, *17*, 2261–2280.
Minvielle, M., and R. D. Garreaud (2011), Projecting Rainfall Changes over the South American Altiplano, *J. Clim.*, *24*(17), 4577–4583, doi: 10.1175/JCLI-D-11–00051.1.
Myers, N., R. A. Mittermeier, C. G. Mittermeier, G. A. B. da Fonseca, and J. Kent (2000), Biodiversity hotspots for conservation priorities, *Nature*, *403*, 853–858.
Nesbitt, S., and A. Anders (2009), Very high resolution precipitation climatologies from the tropical rainfall measuring mission precipitation radar, *Geophys. Res. Lett.*, *36*, L15815, doi:10.1029/2009GL038026.
Paegle, J., and K. C. Mo (1997), Alternating wet and dry conditions over South America during summer, *Mon. Weather Rev.*, *125*, 279–291.
Pepin, E., J. L. Guyot, E. Armijos H. Bazan, P. Fraizy, J. S. Moquet, L. Noriega, W. Lavado, R. Pombosa, and P. Vauchel (2013), Climatic control on eastern Andean denudation rates (Central Cordillera from Ecuador to Bolivia), *J. South Amer. Earth Sci.*, *44*, 85–93. doi:10.1016/ j.jsames.2012.12.010.
Petersen, W., S. W. Nesbitt, R. J. Blakeslee, R. Cifelli, P. Hein, and S. Rutledge (2002), TRMM observations of intraseasonal variability in convective regimes over the Amazon, *J. Clim.*, *15*, 1278–1294.
Póveda, G., L. Jaramillo, and L. F. Vallejo (2014), Seasonal precipitation patterns along pathways of South American low-level jets and aerial rivers, *Water Resour. Res.*, *50*, 98–118, doi:10.1002/2013WR014087.
Romatschke, U., and R. A. Houze Jr. (2010), Extreme summer convection in South America, *J. Clim.*, *23*, 3761–3791.
Satyamurty, P., C. A. Nobre, and P. L. Silva Dias (1998), Tropics-South America, in Karoly DJ, Vincent DG (Org.) Meteorology and hydrology of the southern hemisphere, Boston, *Meteorol. Monogr.*, *49*, 119–139.
Saulo, A. C., M. Nicolini, and S. C. Chou (2000), Model characterization of the South American low-level flow during the 1997–1998 spring-summer season, *Clim. Dyn.*, *16*, 867–881.
Scheel, M. L. M., M. Rohrer, Ch. Huggel, D. Santos Villar, E. Silvestre, and G. J. Huffman (2011), Evaluation of TRMM Multi-satellite Precipitation Analysis (TMPA) performance in the Central Andes region and its dependency on spatial and temporal resolution, *Hydrol. Earth Syst. Sci.*, *15*, 2649–2663.
Uppala, S. M., et al. (2005), The ERA-40 re-analysis, *Q. J. R. Meteorol. Soc.*, *131*, 2961–3012.
Vera C., et al. (2006), Towards a unified view of the American monsoon system, *J. Clim.*, *19*, 4977–5000.
Vuille, M., and C. Ammann (1997), Regional snowfall patterns in the high, arid Andes, *Clim. Change*, *36*, 413–423.
Wang, H., and R. Fu (2002), Cross-equatorial flow and seasonal cycle of precipitation over South America, *J. Clim.*, *15*, 1591–1608.
Zhou, J., and K. M. Lau (1998), Does a monsoon climate exist over South America?, *J. Clim.*, *11*, 1020–1040.
Zulkafli, Z., W. Buytaert, C. Onof, B. Manz, E. Tarnavsky, W. Lavado, and J. L. Guyot (2014), A comparative performance analysis of TRMM 3B42 (TMPA) versions 6 and 7 for hydrological applications over Andean–Amazon river basins, *J. Hydrometeorol.*, *15*(2), 581–592, doi: 10.1175/JHM-D-13-094.1.